Journal of Materials Chemistry B

Accepted Manuscript

ROYAL SOCIETY OF CHEMISTRY

www.rsc.org/materialsB

Size-tunable LDH-protein hybrids toward the optimization of drug nanocarriers

R. Rojas, C. E. Giacomelli*.

INFIQC-CONICET, Departamento de Fisicoquímica, Facultad de Ciencias Químicas, Universidad Nacional de Córdoba, Ciudad Universitaria, 5000 Córdoba, Argentina.

Corresponding author. Tel: +54 351 5353866. Fax: +54 351 4334188. E-mail address: giacomel@fcq.unc.edu.ar.

Abstract

Layered double hydroxides (LDHs) are extensively investigated as drug nanocarriers due to their anion exchange properties and potential capacity to produce enhanced cellular trafficking and targeted delivery. In this work, LDH-protein hybrids with controlled particle size were obtained by modulation of the charge and hydrophobicity of LDH matrixes. In order to do that, bovine serum albumin (BSA) adsorption was studied in LDH matrixes intercalated with chloride and dodecylsulfate in different ratios with its the dependence with pH and ionic strength was determined. Positively charged LDH-Cl matrixes in aqueous solution changed from micro to nano size when adsorbing BSA molecules at pH values higher than the isoelectric point of the protein. On the other hand, the low BSA hybridization with negatively charged LDH-DS matrix was not enough to reduce its particle size. However, a fine tuning of the physicochemical properties of the LDH-Cl matrix by controlled DS^- incorporation and pH and ionic strength conditions allowed LDH-BSA nanohybrids partially intercalated with the surfactant that exhibited colloidal stability at high ionic strength (similar to that of biological fluids).

Keywords

Nanohybrids, electrostatic interactions, steric repulsion, interfacial modification

Introduction

Site-specific delivery of drugs and biomolecules has become an important research area due to the inefficiency of their direct administration and the instability of these agents in biological media[1]. Inorganic vehicles, such as gold, silica or oxide nanoparticles, carbon nanotubes or layered double hydroxides (LDHs) have been investigated as drugs nanocarriers due to their low toxicity, rich functionality and potential capacity to produce enhanced cellular trafficking and targeted delivery[2]. The utility of these nanomaterials as drugs nanocarriers is highly dependent on their capacity to reach the site of therapeutical action from the injection place, avoiding elimination by the reticuloendotelial system, and to produce an effective traffic through the cellular membrane. Particle size and tailored surface properties are of major importance to enhance the colloidal stability and/or increase the circulation time of nanocarriers[1].

In particular, LDH (nano)particles present high interest[3,4] due to their low cytotoxicity[5], high drug loading capacity[6], pH triggered release[7] and drug protection[3], among other advantages. LDHs are bidimensional solids with brucite ($Mg(OH)_2$)-like, positively charged layers that portray anion exchange properties. LDH matrixes can be easily obtained at laboratory scales with simple methods providing a fine tuning of the particle size and enhanced cellular trafficking capability[3,4,8,9]. These matrixes can be intercalated with a wide range of anions, including anti-inflammatory, antimicrobial and anticancer drugs [10–13] and biomolecules (DNA, siRNA or proteins)[3,14–17], which are released under appropriate conditions by different mechanisms, such as anion exchange, weathering and desorption[6].

Proteins are widely used to stabilize emulsions, foams and dispersions by steric forces, preventing the coalescence or coagulation of the dispersed phase (droplets, bubbles or particles)[18]. Then, LDH-protein hybrids are expected to show increased colloidal

stability than the corresponding bare LDH matrixes. Moreover, LDH hybrids with proteins featuring recognition or membrane penetration capabilities may provide additional functionality to LDH-based nanocarriers[19–21]. On this regard, LDH-protein hybrids have been previously studied with heme proteins (hemoglobin, mioglobin and horseradish peroxidase)[22–25], bovine serum albumin [26,27], and enzymes, such as lipases [26], urease [28] or aminopeptidase[29]. In most of these works, the protein maintained their activity after incorporation to the LDH matrix. On the other hand, there are only a few articles aimed at understanding the factors that determine LDH-protein interactions [30], like charge and hydrophobicity of LDH matrixes[31,32].

The reactivity and interfacial properties of LDHs must be tailored to optimize protein adsorption and the interlayer anion plays a major role in this aspect. Chloride and dodecylsulfate are ideal anions to study the customization of LDH properties. The former anion is loosely bonded and easily removed by other anions in solution and chloride intercalated LDHs positively charged particles in a wide pH range and hydrophillic[33]. On the other hand, anionic surfactants, such as dodecylsulfate (DS^-) anions, are attached to LDH surfaces with high affinity due to electrostatic and lateral interactions, leading to the formation of a DS^- monolayer or bilayer depending on the surfactant concentration [34]. As a consequence, the charge and hydrophobicity of LDH matrixes can be modulated from positively charged and hydrophilic to negatively charged and hydrophobic[31,35] by controlling chloride/DS^- anions ratio in LDH matrixes.

This work aims at obtaining LDH-protein nanohybrids and controlling their size distribution in aqueous solution by modulating the charge and hydrophobicity of LDH matrixes, with the long term objective of synthesizing biofunctionalized drug nanocarriers with proper colloidal stability in biological media. The nanohybrids were prepared by bovine serum albumin (BSA) incorporation to Cl^- or DS^- intercalated LDH

matrixes in order to study systematically the effect of the interfacial properties on the hybrids behavior. The effect of pH and ionic strength conditions on the obtained nanohybrids was also determined.

2. Materials and Methods.

2.1. LDH matrixes: Synthesis and characterization.

Chloride (LDH-Cl) and dodecylsulfate (LDH-DS) intercalated Mg-Al-LDH matrixes were prepared by the coprecipitation method at constant pH as described elsewhere[36], the Mg:Al ratio in the starting solution being 3:1. Mg and Al content was determined by atomic absorption spectrometry in a Varian AA240 instrument. The samples were dissolved in HNO_3 and afterwards diluted to meet the calibration range. C, N, and S (CNS) contents were determined using a CHN 2400 Serie II Elemental Analyzer, using cisteine as reference. Thermogravimetric and differential thermal analyses (TG/DTA) were carried out in a Shimadzu DTG 60 instrument, in flowing air at a heating rate of 10 ºC/min. Powder X-Ray diffraction (PXRD) patterns were recorded in a Phillips X'pert Pro instrument using a CuKα lamp (λ= 1.5408 Å) at 40 kV and 40 mA between 5° and 70° (2θ) in step mode (0.05°, 1.2 s). FT-IR spectra were measured in a Bruker IFS28 instrument using KBr pellets (1:100 sample:KBr ratio). Scanning electron microscopy (SEM) images were obtained in a FE-SEM Σigma instrument on samples covered with a Cr layer.

The hydrodynamic apparent diameter (d) and zeta potential (ζ) of the LDH matrixes were determined by dynamic light scattering (DLS) and electrophoretic light scattering (ELS) measurements, respectively, using a Delsa Nano C instrument (Beckman Coulter). Aqueous dispersions of the matrixes (1 g L^{-1}) were prepared and equilibrated for 16 hours and their d and ζ values were determined. These experiments were performed as a function of pH in 0.05 mol L^{-1} NaCl and at pH 9.0 using different

NaCl concentrations. *d* and polydispersity values were calculated from the autocorrelation function ($g^{(2)}$) with the cumulants method, while electrophoretic mobilities were converted to ζ using the Smoluchowski equation.

2.3. LDH-BSA hybrids: Synthesis and characterization .

Stock LDH dispersions (either LDH-Cl or LDH-DS, 3 g L^{-1} in 0.05 mol L^{-1} NaCl), and BSA (2 g L^{-1} in 0.05 mol L NaCl), and NaDS (0.01 mol L^{-1} in 0.05 mol L^{-1} NaCl) solutions were used in the experiments, which were performed at room temperature in all cases.

2.3.1. Effect of the interlayer anion.

LDH-BSA hybrids were prepared by dispersion of the LDH matrixes (either LDH-Cl or LDH-DS, 1.00 g L^{-1}) in 0.05 mol L^{-1} NaCl with increasing BSA concentration (ranging from 0.03 to 1.34 g L^{-1}). These dispersions were equilibrated overnight at 25 ºC (the pH was adjusted before and after equilibration to 9.0±0.2 with 0.2 mol L^{-1} solutions of either NaOH or HCl.) In order to determine BSA adsorbed amount (Γ, g g^{-1}), the protein concentration in the supernatants was measured by UV-Vis spectrophotometry (Shimadzu UV1601, Japan) at λ=279 nm after centrifugation. ζ and *d* values of the LDH-BSA hybrids suspended in aqueous solution were also obtained as previously described.

2.3.2. Effect of the interfacial properties: DS^- anions.

In order to modulate its interfacial properties, LDH-Cl matrix was exchanged with DS^- anions to different extents of its anion exchange capacity (AEC, given by the amount of Al^{3+} ions per unit mass). LDH-Cl dispersions in 0.05 mol L^{-1} NaCl solutions with increasing initial NaDS concentration (up to 6.4 10^{-3} mol L^{-1}, corresponding to 200 % AEC) were equilibrated for 1 hour, obtaining LDH-Cl/DS matrixes. Next, BSA stock solution was added to obtain an overall 0.50 g L^{-1} initial concentration and equilibrated

overnight to obtain LDH-Cl/DS-BSA hybrids. Γ, ζ and d values of both LDH-Cl/DS matrixes and LDH-Cl/DS-BSA hybrids were obtained as previously described.

The nanohybrids obtained at 0 (LDH-Cl-BSA), 50 (LDH-Cl/DS-50-BSA), 100 (LDH-Cl/DS-100-BSA) and 200 (LDH-Cl/DS-200-BSA) %AEC, were separated by centrifugation, washed once with water and finally lyophilized in a Labconco Freezone 6 apparatus. CNS chemical analysis, PXRD patterns, FT-IR spectra as well as SEM images of the hybrids were obtained as previously described.

2.3.3. Effect of the interfacial properties: pH and ionic strength.

In order to study the effect of pH and ionic strength, the synthesis of LDH-Cl-BSA and LDH-Cl/DS-100-BSA hybrids was repeated at different HCl and NaCl concentrations. Γ, ζ and d values were obtained as previously described. Parallel experiments were performed in the absence of BSA to determine the effect of pH and ionic strength on the zeta potential and and particle size of LDH-Cl and LDH-Cl/DS-100 matrixes.

3. Results and discussion.

3.1. LDH matrixes.

The chemical analysis of the samples (Supplementary information Table S1) indicated that a single Mg–Al–LDHs phase was obtained for each matrix with the following chemical formulae: $[Mg_{0.76}Al_{0.24}(OH)_2]Cl_{0.22}(CO_3)_{0.01}\cdot 0.85H_2O$ for LDH–Cl and $[Mg_{0.75}Al_{0.25}(OH)_2]DS_{0.26}\cdot 0.55H_2O$ for LDH–DS. The anion/Al ratio was slightly higher than 1 for LDH-DS, which was assigned to NaDS adsolubilization at the particle surface due to specific adsorption of the surfactant [31,37]. PXRD patterns, FT-IR spectra (Figures 1 and 2) and thermal analysis curves (Supplementary information, Figure S1) of LDH-Cl and LDH-DS matrixes confirmed the presence of pure LDH phases containing Cl^- and DS^- anions, respectively. The PXRD patterns (Figures 1A and 1B) portrayed typical LDH features; narrow and symmetric peaks at 2θ below 30º, and

broad and asymmetric ones above this value. These peaks were indexed in a rhombohedral lattice and the *c* parameters obtained (24.0 and 76.1 Å for LDH-Cl and LDH-DS, respectively) were in good accord with those previously reported for Cl^- and DS^- intercalated LDHs [38,39]. The FT-IR spectra of the matrixes (Figures 2A and 2B) presented bands corresponding to the hydroxilated layers (below 1000 cm^{-1}) and interlayer water (at 1633 and 1658 cm^{-1}, respectively). LDH-DS matrix also presented bands corresponding to CH bending (1469 cm^{-1}), SO_3^- antisymmetric and symmetric stretching (1221 cm^{-1} and 1084 cm^{-1}, respectively) and C-S stretching (634 cm^{-1}) vibrations [40].

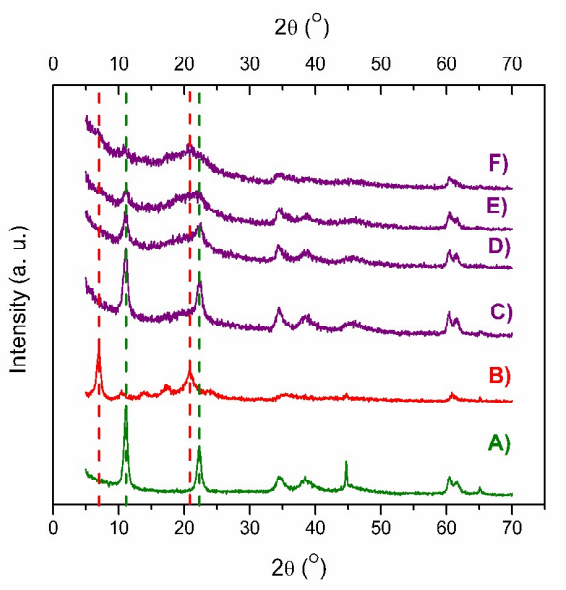

Figure 1. PXRD patterns of LDH-Cl (A), LDH-DS (B), LDH-Cl-BSA (C), LDH-Cl/DS-50-BSA (D), LDH-Cl/DS-100-BSA (E) and LDH-Cl/DS-200-BSA (F) samples.

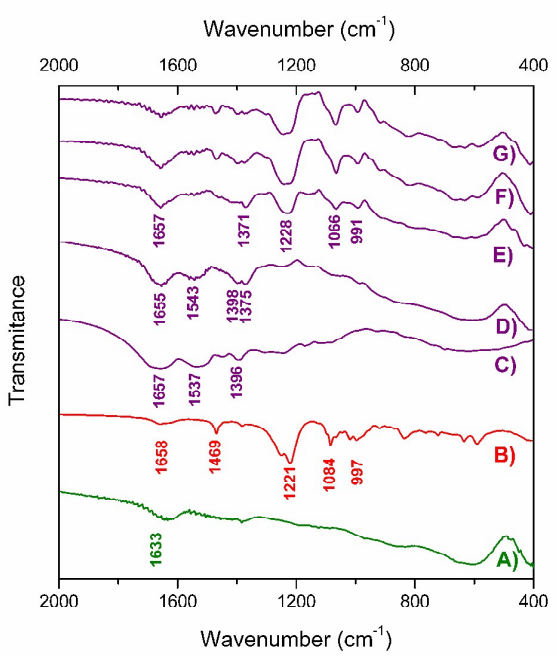

Figure 2. FT-IR spectra of LDH-Cl (A), LDH-DS (B), BSA (C), LDH-Cl-BSA (D), LDH-Cl/DS-50-BSA (E), LDH-Cl/DS-100-BSA (F) and LDH-Cl/DS-200-BSA (G) samples.

The particle size and morphology of the matrixes were characterized by DLS (Supporting Information Figure S2) and SEM images (Figure 3A and 3B). According to DLS measurements, the size of LDH-DS and LDH-Cl particles increased with increasing [NaCl] and they portrayed, at [NaCl]=0.05 mol L^{-1}, d values around 4 μm and 900 nm, respectively. The SEM images of the as-prepared LDH matrixes exposed that they were formed by agglomeration of platelets with irregular shape, sized around 200-300 nm and high diameter to thickness aspect ratio. LDH-Cl matrix (Figure 3A) showed a less compact disposition of their platelets than LDH-DS (Figure 3B), indicating weaker particle-particle interactions.

The different affinity of chloride and DS^- anions was evidenced by the ζ values of LDH-Cl and LDH-DS matrixes. As in previous works [31], ζ values for LDH-DS were almost constant around -25 mV up to 0.15 mol L^{-1} NaCl and in a wide pH range (Supporting Information, Figure S2 and S3) due to the high affinity of DS^- anions for LDH layers [31].

On the other hand, LDH-Cl exhibited a positive charging (Supporting Information, Figures S2 and S3) as corresponds to anions that exclusively present electrostatic interactions with LDHs[31,37]. Only at pH values above 10.5 a drastic ζ decrease was produced, an iep being reached at a pH between 11 and 11.5.

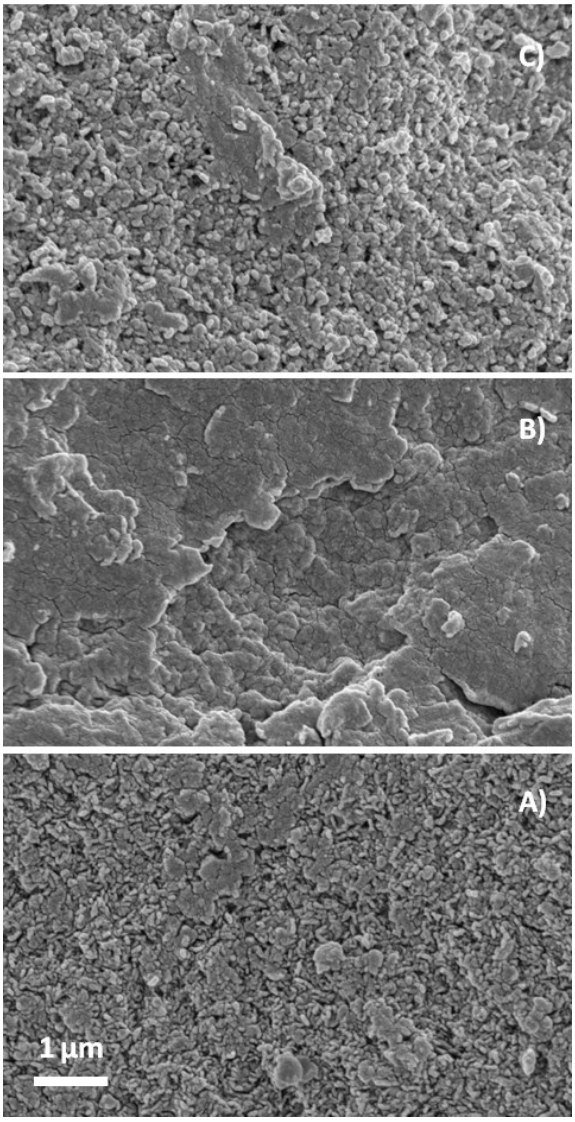

Figure 3. SEM images of LDH-Cl (A), LDH-DS (B) and LDH-Cl/DS-100-BSA (C) samples.

3.2. LDH-BSA hybrids.

BSA hybrids with LDH-Cl and LDH-DS matrixes were obtained in dispersions of increasing protein concentration ($[BSA]_{eq}$) at pH=9.0 and [NaCl]=0.05 mol L^{-1}

(Figure 4). For LDH-Cl, the protein adsorbed amount (Γ) increased steeply at very low protein concentration, indicating the high affinity of BSA for this matrix (Figure 4A). As $[BSA]_{eq}$ increased, Γ reached a plateau value at around 0.25 g g^{-1}, corresponding to the maximum adsorption capacity in these conditions of pH and ionic strength. This result was similar to that obtained by other authors for BSA incorporation to a LDH-lactate matrix [26]. As BSA was incorporated to LDH-Cl, ζ diminished steeply, reaching an isoelectric point (iep) at very low protein concentration and finally a plateau value at -13 mV (Figure 4B). Finally, the hydrodynamic apparent diameter (*d*) of LDH-Cl-BSA hybrids increased as the iep was approached whereas it decreased to 300 nm as ζ becomes increasingly negative (Figure 4C). The PXRD patterns of LDH-Cl-BSA hybrid (Figure 1C) showed the same peaks of LDH-Cl (Figure 1A), indicating that, as stated by An and coworkers [26], BSA intercalation was not produced. Finally, the FT-IR spectra of LDH-Cl-BSA hybrids (Figure 2D) and BSA (Figure 2C) showed similar bands, which confirmed the presence of the protein. In short, the observed change from micro to nano size was the consequence of incorporating BSA molecules on the surface of the LDH-Cl matrix.

On the other hand, BSA incorporation to LDH-DS matrix was below the detection limit pointing to a much lower hybridization capacity of this matrix (Figure 4A). Nevertheless, ζ increased slowly with increasing $[BSA]_{eq}$ and reached a steady value similar to that of LDH-Cl-BSA (Figure 4B), which indicated that the protein was also incorporated to LDH-DS. On the contrary, the low hybridization leaded to negligible changes in the particle size (Figure 4C).

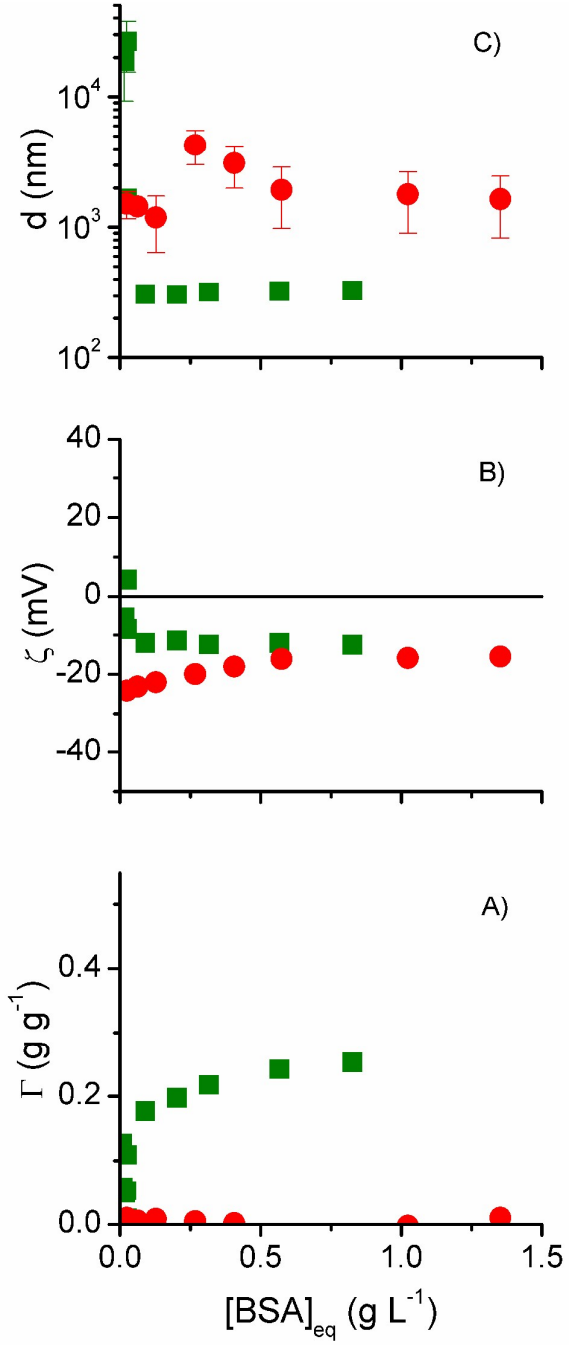

Figure 4 Γ: BSA adsorbed amount (A), ζ: zeta potential (B) and d: hydrodynamic apparent diameter (C) vs. BSA equilibrium concentration ([BSA]$_{eq}$) curves of hybrids obtained from LDH-Cl (squares) and LDH-DS (circles) matrixes dispersed in aqueous solution (pH 9.0, 0.05 mol L^{-1} NaCl solution). Error bars represent standard deviation determined from three determinations.

The hybridization was mainly due to the electrostatic interactions between the matrixes and BSA. At pH 9.0, LDH-Cl and LDH-DS were positively and negatively charged, respectively, while BSA was negatively charged (iep 4.7 [41]), leading to a

higher affinity for the former. The protein layer on the LDH-Cl matrix determined the electrokinetic behavior of the LDH-Cl-BSA hybrid, as widely observed with metal (hydr)oxides, such as alumina, silica, zirconia or titania [41,42]. Due to the high affinity of BSA for LDH-Cl, the protein molecules were able to disaggregate the small units that form the LDH particles. On the other hand, protein molecules are also incorporated to solid surfaces in adverse electrostatic conditions, especially in the case of proteins with a high capacity of undergoing conformational changes, or "soft" proteins, such as BSA [43]. Thus, although BSA exhibited lower affinity for LDH-DS matrix than for LDH-Cl, there was a small incorporation, as reflected by ζ variation. However, the low BSA hybridization was not enough to produce disaggregation of the LDH-DS particles.

3.3. Effect of the interfacial properties: DS^- anions.

In order to produce a fine tuning of the physicochemical properties of the LDH matrixes and produce LDH/BSA nanohybrids intercalated with DS^- anions, LDH-Cl was exchanged with the latter, obtaining LDH-Cl/DS matrixes that were afterwards modified with BSA to obtain LDH-Cl/DS-BSA hybrids. In these model systems, LDH/BSA nanohybrids represented biofunctionalized drug nanocarriers that may be used in targeted delivery while DS^- mimicked anionic amphiphilic drugs. Γ, ζ and d values were registered as a function of %AEC for both LDH-Cl/DS matrixes and LDH-Cl/DS-BSA hybrids (Figure 5). The LDH-Cl/DS-BSA hybrids were also characterized by PXRD patterns (Figure 1 D-F), FT-IR spectra (Figure 2 E-G) and CNS content determinations (Figure 6).

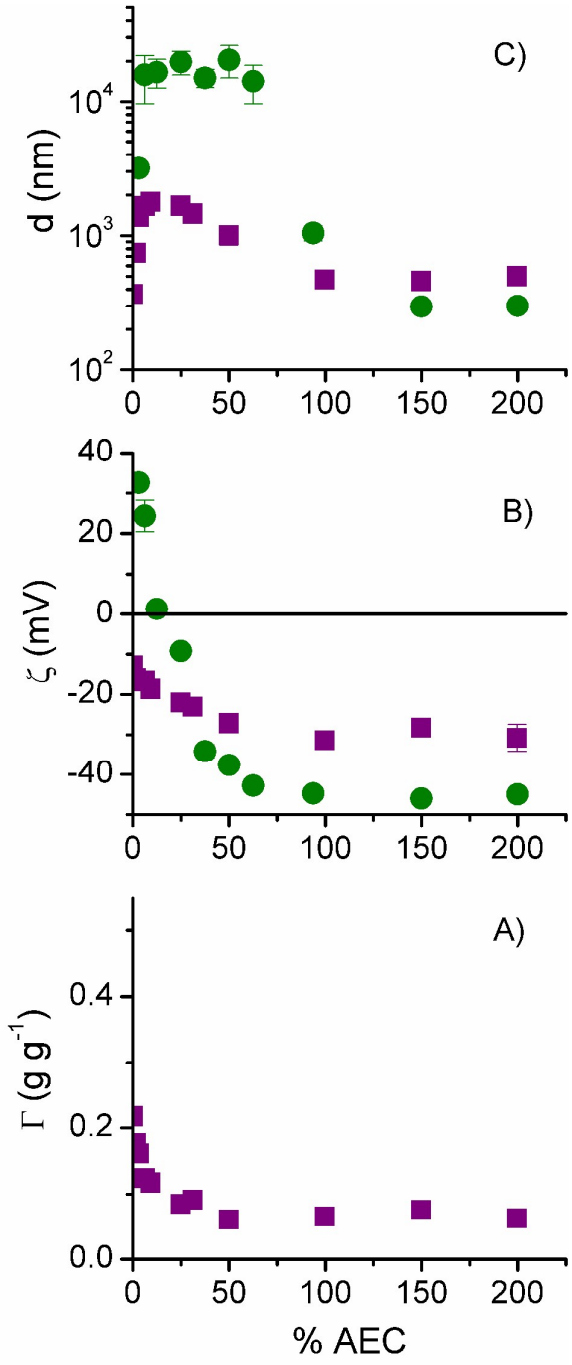

Figure 5. Γ: BSA adsorbed amount (A), ζ: zeta potential (B) and d: hydrodynamic apparent diameter (C) vs. the percentage of the anion exchanged capacity (%AEC) curves for LDH-Cl/DS matrixes (circles) and LDH-Cl/DS-BSA hybrids (squares) dispersed in aqueous solution (pH 9.0, 0.05 mol L^{-1} NaCl, 0.5 g L^{-1} BSA solution. Error bars represent standard deviation determined from three determinations.

With respect to LDH-Cl/DS matrixes, their particle size increased steeply to tens of micrometers at low %AEC and decreased down to hundreds of nanometers upon further addition of DS^- anions. On the other hand, ζ vs. %AEC curves showed a steep

decrease at low %AEC, reaching a constant negative value at %AEC higher than 50. As previously indicated [31], DS^- anions attached with high affinity to LDH surfaces, leading to the formation of a monolayer that compensated (at around 25% AEC) the positive charge and increased the surface hydrophobicity (the water contact angle changed from 32^o to 71^o in going from LDH-Cl to LDH-DS). At higher exchange ratios, a bilayer was formed, reverting the particle charge and diminishing the hydrophobic character of the surface[31,34]. Together with the bilayer formation DS^- anions were also intercalated in the interlayer region[31].

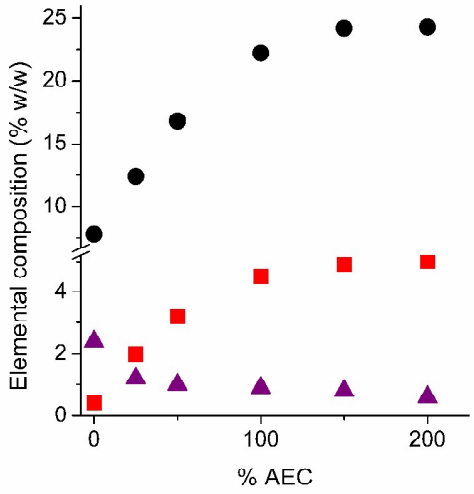

Figure 6. Carbon (circles), nitrogen (triangles), and sulfur (squares) weight/weight percentage (% w/w) of LDH-Cl/DS-BSA hybrids as a function of the anion exchange capacity (%AEC).

As expected, BSA incorporation to LDH-Cl/DS matrixes diminished as %AEC increased, although Γ at % AEC=200 was still 20% of the adsorbed amount at [NaDS]=0 (Figure 5A). At %AEC=0, BSA adsorption reverted the positive ζ values of LDH-Cl matrix (Figure 5B) and increasing %AEC further increased the negative ζ values of LDH-Cl/DS-BSA hybrids from -10 mV to -30 mV. Similarly to that for LDH-Cl/DS matrixes, the formation of the DS^- anions bilayer increased the particle disaggregation at high %AEC (Figure 5C) while the formation of the DS^- monolayer induced particle aggregation even in the presence of BSA at low %AEC values.

Nevertheless, the particle size increase was less pronounced for LDH-Cl/DS-BSA hybrids than for LDH-Cl/DS matrixes due to the increased steric repulsions produced by the adsorbed BSA. Consequently, the particle size of LDH-Cl matrixes can be tuned from micro to nano by adding BSA and/or DS^- anions due to electrostatic and/or steric repulsions.

PXRD patterns of the LDH-Cl/DS-BSA hybrids (Figure 1D-F) showed that the (0 0 *l*) peaks observed in LDH-Cl diminished their intensity as %AEC increased and small peaks of a DS^- intercalated phase were observed for LDH-Cl/DS-100-BSA and LDH-Cl/DS-200-BSA. As discussed elsewhere, depending on the added amount of DS^-, the surfactant was either adsorbed (%AEC < 25) or adsorbed and intercalated in the interlayer of the particles (%AEC > 25) before BSA incorporation [31]. The FT-IR spectra of these nanohybrids (Figure 2E-G) indicated that the intensity of the BSA and DS^- bands decreased and increased, respectively, by raising %AEC. The chemical composition of the samples (Figure 6) reflected these trends, as the N content of the samples diminished from LDH-Cl-BSA to LDH-Cl/DS-200-BSA hybrids while C and S contents increased. Thus, the DS/Al ratio increased with increasing %AEC, reaching around 0.7 for LDH-Cl/DS-100-BSA and LDH-Cl/DS-200-BSA (Supporting information, Table S1). This DS/Al ratio confirmed that DS^- anions were not exclusively placed at the particle surface, but they were also intercalated between the layers. The SEM images of LDH-Cl/DS-BSA hybrids (Figure 3C) showed a loose disposition of their platelets, similar to that of the LDH-Cl, indicating weak particle-particle interactions.

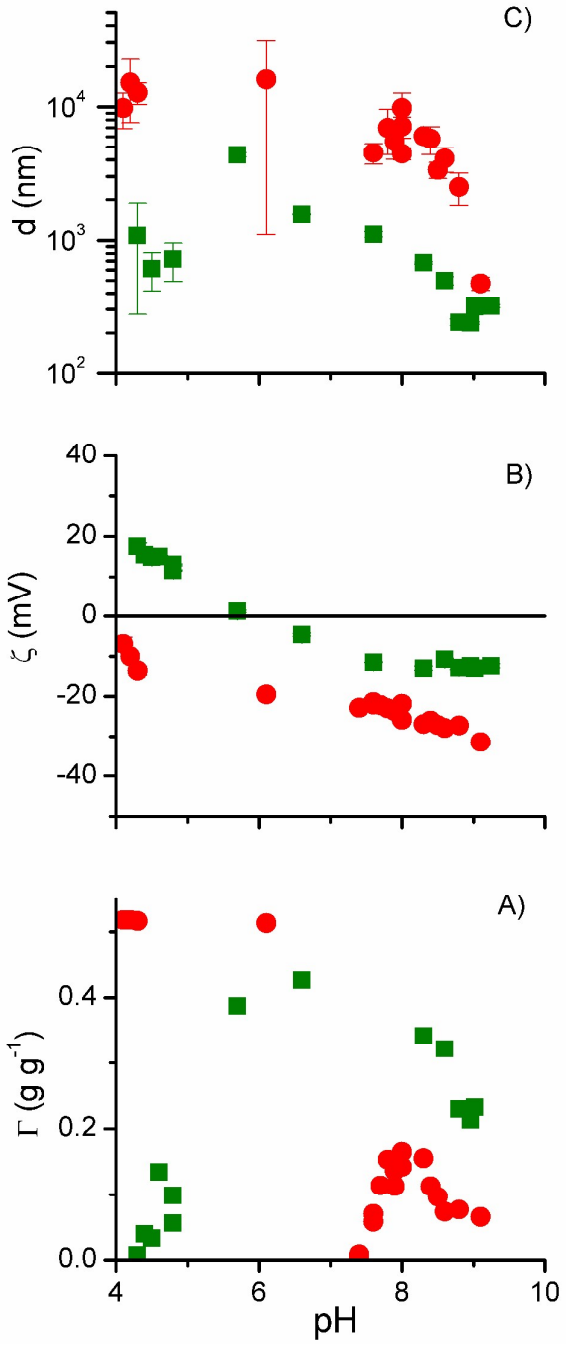

Figure 7. Γ: BSA adsorbed amount (A), ζ: zeta potential (B) and d: hydrodynamic apparent diameter (C) vs. pH curves for LDH-Cl-BSA (squares) and LDH-Cl/DS-100-BSA (circles) hybrids dispersed in aqueous solution (0.05 mol L^{-1} NaCl, 0.5 g L^{-1} BSA solution). Error bars represent standard deviation determined from three determinations.

3.4. Effect of pH and NaCl concentration.

The solution pH is the most important factor to control protein adsorption on oxides[41] and clays[44], as it affects the charge of both the protein and the sorbent surface. *Γ, ζ, and d* of LDH-Cl/DS-0-BSA and LDH-Cl/DS-100-BSA nanohybrids showed a strong

dependence with pH (Figure 7). In the first case, the pH effect followed the electrostatic interaction between the matrix and the protein since the maximum adsorbed amount agreed with the iep of both the protein and the hybrids and diminished at both sides, as observed with metal (hydroxides)[42,45]. This electrostatic interaction controlled the particle size and *d* increased with decreasing particle charge, reaching a maximum at the iep. On the other hand, the pH effect was more complex for hybrids obtained from LDH-Cl/DS-100 matrixes: Γ increased from 0.07 to 0.17 g g^{-1} as pH decreased from 9 to 8, then abruptly decreased, being negligible at pH=7.5 and finally increased steeply at lower pH values to 0.5 g g^{-1}, corresponding to a complete BSA removal from the aqueous solution. This behavior was not ruled by electrostatic interactions between the matrix and the protein, as observed by the ζ vs. pH curve, which did not reach the iep. However, ζ values affected the particle size, which increased from a few hundred nm to a few tens μm as the former diminished. The complex Γ vs. pH profiles measured in the presence of DS^- anions indicated that multiple processes should be considered, such as BSA and LDH charging, DS^- interactions with the LDH surface and BSA, LDH weathering and BSA denaturalization[46,47].

Finally, the effect of ionic strength on LDH-BSA nanohybrids with LDH-Cl/DS-0 and LDH-Cl/DS-100 matrixes was also explored (Figure 8). As expected for attractive and repulsive electrostatic interactions, Γ diminished with increasing [NaCl] for LDH-Cl/DS-0 matrix while it increased for LDH-Cl/DS-100, both variations being quite subtle. Cl^- anions competed for positively charged binding sites on LDH-Cl matrixes whereas they increased the charge screening and diminished the electrostatic repulsions between BSA and LDH-Cl/DS-100 matrix. On the other hand, ζ and *d* remained almost constant with increasing [NaCl] in both cases, d values being lower than 500 nm in all cases. It is important to note that according to ASTM (American Society for Testing and

Materials) standard for stability of colloidal suspension, a positive or negative zeta potential between 30 and 40 mV is indicative of a substance with moderate stability while absolute values above 40 mV are associated to high stability [48].

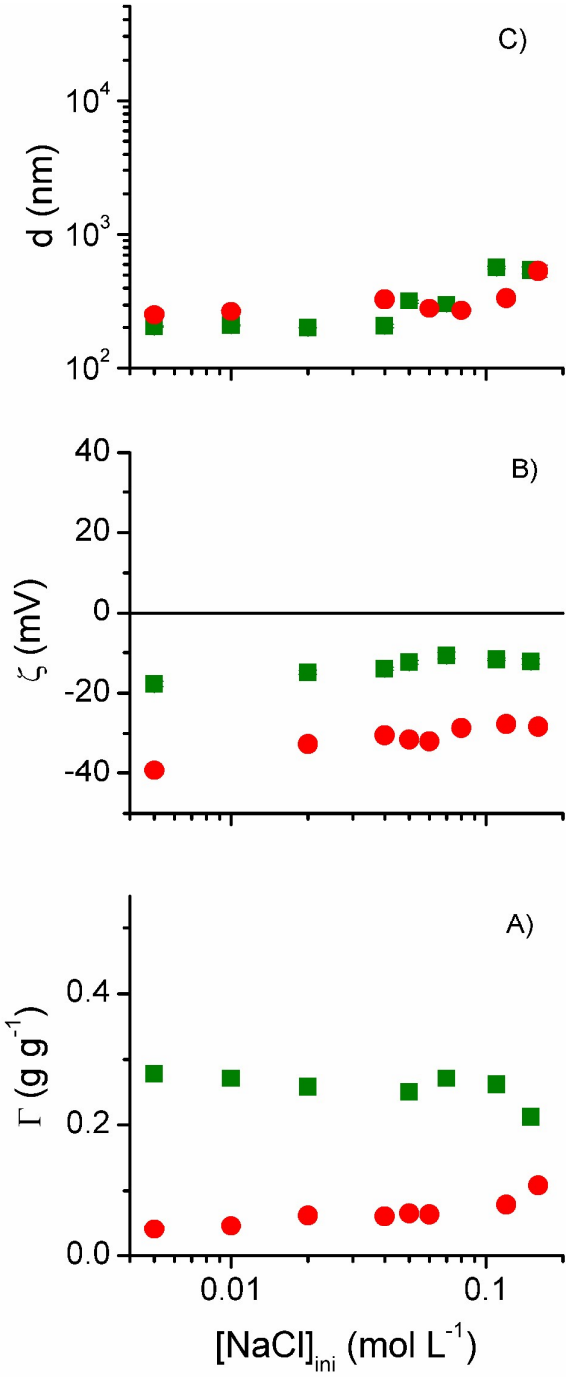

Figure 8. BSA adsorbed amount (A), ζ: zeta potential (B) and d: hydrodynamic apparent diameter (C) vs. the initial NaCl concentration ([NaCl]$_{ini}$) curves for LDH-Cl-BSA (squares) and LDH-Cl/DS-100-BSA (circles) hybrids dispersed in aqueous solution (pH 9.0, 0.5 g L^{-1} BSA solution). Error bars represent standard deviation determined from three determinations.

Compared to the effect of ionic strength of LDH-Cl and LDH-DS matrixes (Supporting information, Figure S2), the colloidal stability of both LDH-Cl/DS matrixes and LDH-Cl/DS-BSA matrixes was increased, being especially remarkable at high ionic strength values, similar to that of biological fluids. This stabilization was achieved by adsorption of either DS^- anions, BSA or both (Supplementary information, Figure S2). Therefore, LDH hybridization with proteins, such as BSA, seems a suitable approach to produce nanocarriers of either hydrophobic or hydrophillic drugs[49] with increased colloidal stability and enhanced functionality.

Conclusions.

LDH-BSA nanohybrids with tunable size and increased colloidal stability were obtained by control of the interfacial properties of LDH matrixes and medium conditions, like pH and ionic strength. Optimized conditions involved modification of chloride intercalated matrixes with anionic surfactants or proteins, their incorporation being determined mainly by electrostatic interactions. With a fine tuning of the synthesis conditions, LDH-BSA nanohybrids containing either chloride or DS^- anions were obtained, which indicated that BSA can be incorporated to nanocarriers loaded with drugs featuring different physicochemical properties. These drug nanocarriers exhibited with increased colloidal stability and additional functionality is envisaged by modulating the interaction of LDH matrixes with recognition proteins such as antigens.

Acknowledgements.

Economic support by SeCyT-UNC project number 05/C585, FONCyT, project numbers 12/0634 and 10/2116, and CONICET, PIP 11220120100575, are gratefully acknowledged.

Supporting Information Available.

The following files are available free of charge: a word document containing Table S1: Chemical analysis of LDH-Cl and LDH-DS matrixes and LDH-Cl/DS-BSA hybrids, Figure S1: Thermal analysis and Figure S2 and S3: d and ζ dependence with pH and [NaCl] curves of LDH-Cl and LDH-DS matrixes.

References.

1 Y. Li, J. Wang, M. G. Wientjes and J. L.-S. Au, *Adv. Drug Deliv. Rev.*, 2012, **64**, 29–39.

2 S. Li, J. Li, C. J. Wang, Q. Wang, M. Z. Cader, J. Lu, D. G. Evans, X. Duan and D. O'Hare, *J. Mater. Chem. B*, 2013, **1**, 61.

3 K. Ladewig, M. Niebert, Z. P. Xu, P. P. Gray and G. Q. M. Lu, *Biomaterials*, 2010, **31**, 1821–9.

4 Z. P. Xu, G. Stevenson, C.-Q. Lu and G. Q. M. Lu, *J. Phys. Chem. B*, 2006, **110**, 16923–9.

5 S.-J. Choi, J.-M. Oh, T. Park and J.-H. Choy, *J Nanosci. Nanotech.*, 2007, **7**, 4017–4020.

6 R. Rojas, M. C. Palena, A. F. Jimenez-Kairuz, R. H. Manzo and C. E. Giacomelli, *Appl. Clay Sci.*, 2012, **62-63**, 15–20.

7 L. Wang, H. Xing, S. Zhang, Q. Ren, L. Pan, K. Zhang, W. Bu, X. Zheng, L. Zhou, W. Peng, Y. Hua and J. Shi, *Biomaterials*, 2013, **34**, 3390–401.

8 M. Chen, H. M. Cooper, J. Z. Zhou, P. F. Bartlett and Z. P. Xu, *J. Colloid Interface Sci.*, 2013, **390**, 275–81.

9 H.-E. Chung, D.-H. Park, J.-H. Choy and S.-J. Choi, *Appl. Clay Sci.*, 2012, **65-66**, 24–30.

10 V. Rives, M. Del Arco and C. Martín, *J. Control. Release*, 2013, **169**, 28–39.

11 U. Costantino, V. Bugatti, G. Gorrasi, F. Montanari, M. Nocchetti, L. Tammaro and V. Vittoria, *ACS Appl. Mater. Interfaces*, 2009, **1**, 668–77.

12 V. Rives, M. del Arco and C. Martín, *Appl. Clay Sci.*, 2014, **88-89**, 239–269.

13 R. Ma, Z. Wang, L. Yan and G. Zhu, *J. Mater. Chem. B*, 2014, **2**, 4868–4875.

14 K. Ladewig, M. Niebert, Z. P. Xu, P. P. Gray and G. Q. (Max) Lu, *Appl. Clay Sci.*, 2010, **48**, 280–289.

15 Y. Wong, K. Markham, Z. P. Xu, M. Chen, G. Q. Max Lu, P. F. Bartlett and H. M. Cooper, *Biomaterials*, 2010, **31**, 8770–9.

16 Z. Gu, A. C. Thomas, Z. P. Xu, J. H. Campbell, G. Qing and M. Lu, *Chem. Mater.*, 2008, 3715–3722.

17 A. Li, L. Qin, W. Wang, R. Zhu, Y. Yu, H. Liu and S. Wang, *Biomaterials*, 2011, **32**, 469–77.

18 P. J. Hailing and P. Walstra, *C R C Crit. Rev. Food Sci. Nutr.*, 1981, **15**, 155–203.

19 A. L. Z. Lee, Y. Wang, W.-H. Ye, H. S. Yoon, S. Y. Chan and Y.-Y. Yang, *Biomaterials*, 2008, **29**, 1224–32.

20 C. Gunawan, M. Lim, C. P. Marquis and R. Amal, *J. Mater. Chem. B*, 2014, **2**, 2060.

21 B. Gupta, T. S. Levchenko and V. P. Torchilin, *Adv. Drug Deliv. Rev.*, 2005, **57**, 637–51.

22 K. Charradi, C. Forano, V. Prevot, D. Madern, A. Ben Haj Amara and C. Mousty, *Langmuir*, 2010, **26**, 9997–10004.

23 X. Chen, C. Fu, Y. Wang, W. Yang and D. G. Evans, *Biosens. Bioelectron.*, 2008, **24**, 356–61.

24 F. Bellezza, A. Cipiciani, L. Latterini, T. Posati and P. Sassi, *Langmuir*, 2009, **25**, 10918–24.

25 X. Kong, X. Rao, J. Han, M. Wei and X. Duan, *Biosens. Bioelectron.*, 2010, **26**, 549–54.

26 Z. An, S. Lu, J. He and Y. Wang, *Langmuir*, 2009, **25**, 10704–10.

27 T. Zhang, Y. Zhou, M. He, Y. Zhu, X. Bu and Y. Wang, *Chem. Eng. J.*, 2013, **219**, 278–285.

28 S. Vial, V. Prevot, F. Leroux and C. Forano, *Microporous Mesoporous Mater.*, 2008, **107**, 190–201.

29 S. T. Frey, S. L. Guilmet, R. G. Egan, A. Bennett, S. R. Soltau and R. C. Holz, *ACS Appl. Mater. Interfaces*, 2010, **2**, 2828–32.

30 K. Ralla, U. Sohling, K. Suck, F. Sander, C. Kasper, F. Ruf and T. Scheper, *Colloids Surf. B. Biointerfaces*, 2011, **87**, 217–25.

31 R. Rojas, F. Bruna, C. P. de Pauli, M. Á. Ulibarri and C. E. Giacomelli, *J. Colloid Interf. Sci.*, 2011, **359**, 136–141.

32 A. Pattammattel, I. K. Deshapriya, R. Chowdhury and C. V Kumar, *Langmuir*, 2013, **29**, 2971–2981.

33 R. Rojas Delgado, M. Arandigoyen Vidaurre, C. P. De Pauli, M. A. Ulibarri and M. J. Avena, *J. Colloid Interf. Sci.*, 2004, **280**, 431–41.

34 P. Pavan, E. Crepaldi and J. Valim, *J. Colloid Interf. Sci.*, 2000, **229**, 346–352.

35 Z. P. Xu, Y. Jin, S. Liu, Z. P. Hao and G. Q. M. Lu, *J. Colloid Interf. Sci.*, 2008, **326**, 522–9.

36 J. He, M. Wei, Y.-G. Kang, D. G. Evans and X. Duan, in *Layered Double Hydroxides*, eds. D. G. Evans and X. Duan, Springer-Verlag, Berlin, 2006, pp. 89–119.

37 R. Rojas and C. E. Giacomelli, *Colloids Surf. A Physicochem. Eng. Asp.*, 2013, **419**, 166–173.

38 P. Wu, T. Wu, W. He, L. Sun, Y. Li and D. Sun, *Colloids Surfaces A Physicochem. Eng. Asp.*, 2013, **436**, 726–731.

39 V. A. Drits and A. S. Bookin, in *Layered Double hydroxides: Present and Future*, ed. V. Rives, Nova Science, New York, 2001, pp. 39–92.

40 C. Yilmaz, U. Unal and H. Yagci Acar, *J. Solid State Chem.*, 2012, **187**, 295–299.

41 C. E. Giacomelli, M. J. Avena and C. P. De Pauli, *J. Colloid Interf. Sci.*, 1997, **395**, 387–395.

42 K. Rezwan, A. R. Studart, J. Vörös and L. J. Gauckler, *J. Phys. Chem. B*, 2005, **109**, 14469–74.

43 W. Norde, J. Buijs and H. Lyklema, in *Fundamentals of Interface and Colloid Science, Volume V*, ed. J. Lyklema, Elsevier, Amsterdam, 2005, vol. 12.

44 W. H. Yu, N. Li, D. S. Tong, C. H. Zhou, C. X. (Cynthia) Lin and C. Y. Xu, *Appl. Clay Sci.*, 2013, **80-81**, 443–452.

45 K. Rezwan, L. P. Meier, M. Rezwan, J. Vo, M. Textor and L. J. Gauckler, *Langmuir*, 2004, 10055–10061.

46 T. Chakraborty, I. Chakraborty, S. P. Moulik and S. Ghosh, *Langmuir*, 2009, **25**, 3062–74.

47 D. Otzen, *Biochim. Biophys. Acta*, 2011, **1814**, 562–91.

48 K. Krishnamoorthy, M. Veerapandian, K. Yun and S. J. Kim, *Carbon N. Y.*, 2013, **53**, 38–49.

49 R. Rojas, A. F. Jimenez-Kairuz, R. H. Manzo and C. E. Giacomelli, *Colloids Surfaces A Physicochem. Eng. Asp.*, 2014, **463**, 37–43.

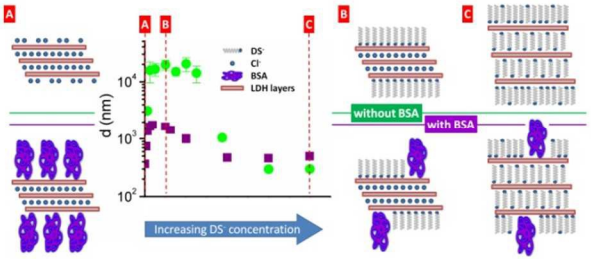

Stabilization of LDH nanoparticles containing chloride and dodecylsulfate with BSA points to optimized drug nanocarriers based on these solids.